

Powder Metallurgical Manufacturing of Ti-Nb alloys Using Coarse Nb Powders

D. M. C. dos Santos^a , F. Signor^a , A.D. Schneider^b , C. R. Bender^c , P. H. Mareze^a , N.F. Daudt^a 

^aUniversidade Federal de Santa Maria (UFSM), Programa de Pós-graduação em Engenharia Mecânica (PGMEC), Santa Maria, RS, Brasil.

^bUniversidade Federal de Santa Maria (UFSM), Programa de Pós-graduação em Física (PGFISICA), Santa Maria, RS, Brasil.

^cUniversidade Federal de Santa Maria (UFSM), Programa de Pós-graduação em Química (PPGQ), Santa Maria, RS, Brasil.

Received: November 03, 2023; Revised: December 21, 2023; Accepted: January 24, 2024

Powder metallurgy is an attractive method for cost effective production of near net shape Ti-Nb alloys, and, when elemental powders and coarse HDH powders are used, a higher flexibility in alloy composition and low processing costs can be achieved. In this study, manufacturing of ($\alpha+\beta$) Ti-Nb alloys by powder metallurgical techniques using coarse HDH Nb ($D_{50} = 110 \mu\text{m}$ and $D_{90} = 255 \mu\text{m}$) and HDH Ti ($D_{50} = 22.6 \mu\text{m}$) powders as starting materials was described. Tape casting was applied for the production of porous sheets while warm compaction of Metal Injection Molding (MIM) feedstock was applied for the production of dense parts. Microstructural and mechanical tests were employed to investigate the effect of coarse Nb powders on the sintering behavior and mechanical properties. Tape casting enabled to produce porous sheets of Ti16Nb alloy with an interconnected porosity varying from 14 – 31 vol.%. Warm compaction enabled to produce Ti-Nb parts with less than 2% porosity and Yield strength in compression of 975-1100 MPa, which is similar to the values reported for Ti-Nb based alloys produced by powder metallurgy of finer powders. A dynamic Young's Modulus of 37-52 GPa, significantly lower than that of cp-Ti was achieved. These results might provide guidelines for the use of coarse Nb powders as starting materials for the powder metallurgical development of low-cost Ti-Nb based alloys.

Keywords: *Sintering, Ti-Nb alloys, MIM, tape casting.*

1. Introduction

In the past 50 years, titanium-based alloys have been investigated due their outstanding properties such as high specific strength, corrosion resistance, creep resistance and their wide range of operating temperatures¹. Ti alloys exhibit an allotropic transformation which enables to produce alloys with different microstructures and properties. So that Ti alloys have been used for a large scope of application such as aerospace structures², naval industry³ and biomedical implants^{4,5}. Currently, Ti-6Al-4V is the most widely used Ti-based alloy for load-bearing implants and aerospace applications. Ti-6Al-4V is ($\alpha+\beta$) type alloy which provides a good combination of strength and creep resistance. However, studies have shown that the release of aluminum and vanadium might cause neurological diseases^{6,7}, in addition there is a large mismatch between Young's modulus of Ti-6Al-4V alloy and human bone which can cause stress shield effect, hindering the osseointegration of the implant⁸.

Ti-Nb alloys have been reported as promising material for the next generation of biomedical implants, since they have the potential to overcome the toxicity and mechanical incompatibility issues associated to the CrCo, stainless steel and Ti-6Al-4V alloys, which are currently the most used alloys for load-bearing implants^{5,9,10}. Niobium is a β stabilizer, so that the amount of niobium can be adjusted

to produce ($\alpha+\beta$) or β type alloys^{9,11,12}. By adding Nb, Ti alloys with higher corrosion resistance¹³⁻¹⁵, lower Young's modulus^{9,14,16} and even superelasticity and shape memory properties^{17,18} can be achieved.

In the case of fabrication of Ti based alloys such as Ti-Nb alloys, the high melting point and affinity of Ti for oxygen requires special furnace and controlled atmosphere for casting; the low ductility hinders their processing by traditional metal forming; and the high cutting temperature and high tool wear makes machining extremely difficult leading to high production and machining costs¹⁹. Therefore, Ti based alloys have attracted attention for powder metallurgical processing. Powder metallurgy has several advantages for Ti alloys manufacturing such as enabling the manufacture of complex parts with high mechanical properties, allowing the reduction of overall weight through the manufacture of complex or porous structures, using a smaller amount of raw material and producing a smaller amount of scrap²⁰.

Powder metallurgical manufacturing of Ti-Nb parts has already been reported in the literature^{5,12,21,22}. For demonstration, Sharma et al.²³ produced β -Ti alloys by mechanical alloying of titanium hydride and Nb elemental powders followed by spark plasma sintering. Terayma et al.²⁴ produced Ti-Nb based shape memory alloys by powder metallurgy: they obtained a Ti-Nb based alloy consisting of α and β phases by mechanical alloying of elemental powders and spark plasma sintering.

*e-mail: natalia.daudt@ufsm.br

Metal Injection Molding^{5,21,25} and tape casting²² have also been applied for production of ($\alpha + \beta$) and β type Ti-Nb alloys using elemental powders. Metal injection molding (MIM) enables the production of near net shape parts with complex geometries with a high degree of material utilization, MIM can contribute to the cost-effective fabrication of Ti-Nb based implants^{12,25,26}. While tape casting is an attractive route for production of porous titanium alloys for electrochemical application^{27,28}.

Pre-alloyed or elemental powders can be used for powder metallurgical fabrication of Ti-Nb alloys. The use of elemental powders increases the composition flexibility once different mixes of elemental powders can be used. Furthermore, the availability of Ti-based pre-alloyed powders is restricted to commercial alloys. So that, pre-alloyed powders of Ti-Nb based alloys must be manufactured in small batches which increases processing costs and energy consumption. In the case of Nb powders, there are few suppliers available. The Brazilian Mining Company, CBMM, is the world's leading supplier of Nb products. CBMM main product is ferroniobium which is produced by aluminothermic reduction, followed by pure niobium ingots produced by electron beam refining of ferroniobium²⁹. Nb powders are only produced at small scale at CBMM by HDH of Nb pellets. Hydrogenation/mill/dehydrogenation procedures can be applied to obtain fine Nb particles with less than 1 μm , the finer the particles, the longer milling time and the higher the energy required³⁰. Currently, there are also some suppliers of spherical Nb powders for MIM and additive manufacturing obtained by plasma atomization, however the cost of these powders is considerably high.

In this study, we investigate the powder metallurgical fabrication of Ti-Nb based alloys using lower cost elemental powders: HDH titanium and coarse HDH niobium. Two powder metallurgical routes were tested: tape casting for production of porous sheets and warm compaction of MIM feedstocks for production of dense parts.

2. Experimental

HDH Ti powders (99.5%, $D_{10} = 10.9 \mu\text{m}$, $D_{50} = 22.6 \mu\text{m}$, $D_{90} = 44.4 \mu\text{m}$) supplied by Alfa Aesar (USA) and acicular

Nb powders with particle size varying from few μm to mm produced by HDH of Nb pellets (CBMM, Brazil) were used as starting metal powders. In this study two particles range of Nb particles ($D_{10} = 47.7 \mu\text{m}$, $D_{50} = 109.7 \mu\text{m}$, $D_{90} = 180.7 \mu\text{m}$) and ($D_{10} = 74.2 \mu\text{m}$, $D_{50} = 255.2 \mu\text{m}$, $D_{90} = 410.9 \mu\text{m}$) obtained by sieving were tested. Tape casting and warm compaction of MIM feedstocks were employed for powder metallurgical manufacturing of Ti-Nb based alloys. Figure 1 shows the morphology of the starting Ti and Nb powders. Warm compaction was used instead of MIM because it enables parts to be fabricated with small amount of feedstocks, avoiding the need of large amount of feedstocks that is required for MIM experiments. In addition, warm compaction and MIM have similar principle: the feedstock is heated above melting temperature of the binder system and molded under pressure. Similar approaches have been reported in the literature³¹⁻³³.

For tape casting, alcohol-based slurries were produced by mixing the metal powders (80 wt.%), isopropanol (18 wt.%) and ethycellulose (1 wt.%) and PEG (1 wt.%). Powder loading was composed of 84 wt.% Ti and 16 wt.% Nb to ensure a formation of ($\alpha + \beta$)-type alloy. The Ti16Nb tapes were produced in a manual tape casting line, the position of doctor blade was adjusted to obtain tapes of ca. 800 μm thickness in the green state. Green tapes were cut in 1 mm x 5 mm pieces and placed in an oven at 60 °C for 60 minutes for solvent evaporation. Thermal debinding and sintering were performed in a high vacuum furnace. For thermal debinding, the samples were heated up with 1 °C/min to 500 °C held at this temperature for 30 minutes. Sintering was performed at 900, 1000, 1100 and 1200 °C with dwell time of 180 minutes. A maximal sintering temperature of 1200 °C was applied to avoid carbide precipitation²².

MIM feedstocks were composed of the metal powders mixture and the binder system. The binder system consisted of 70 vol.% paraffin wax (Sigma-Aldrich, Brazil), 25 vol.% polyethylene (PEAD, Braskem, Germany) and 5 vol.% stearic acid (Sigma-Aldrich, Brazil). MIM feedstocks were produced by mixing powders and the binder system at 160 °C under mechanical stirring.

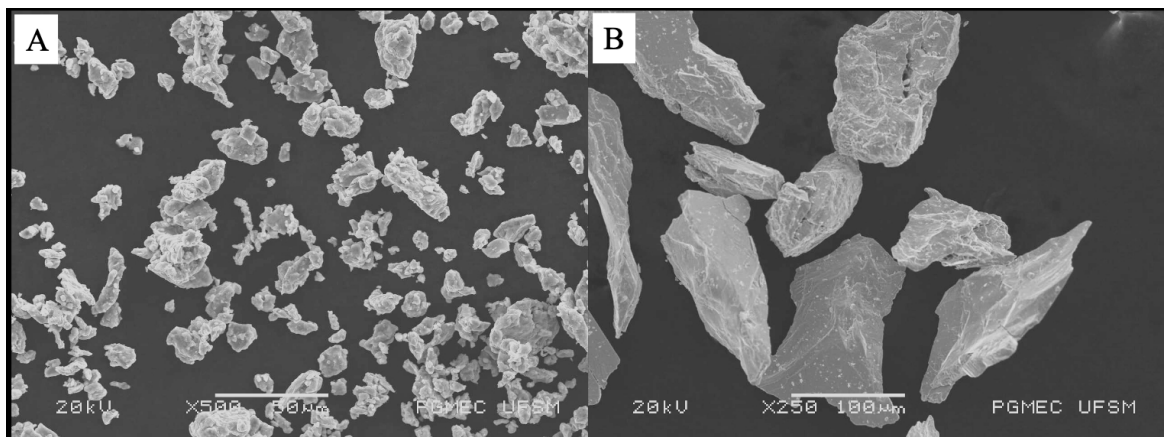


Figure 1. SEM images of (A)Ti and (B) Nb powders.

Green parts were produced by warm compaction of MIM feedstocks following the procedures described elsewhere^{31,32}, which basically consist of adding the MIM feedstock to a die of 11 mm diameter – adjusting the amount of feedstock to obtain green parts of ca. 19 mm height - and then compacting the MIM feedstock by applying a uniaxial pressure of 110 MPa, at 150 °C for 120 s. A laboratory press equipped with electrically heated tool was used (Buehler, Brazil). After warm compaction, the samples were immersed in *n*-hexane bath (50 °C, 24 h) to remove paraffin wax and stearic acid. Thermal debinding and sintering were performed in a high vacuum furnace. The samples were heated up with 1 °C/min to 500 °C held at this temperature for 120 minutes to remove the binder and then sintering was performed at 1200 °C for 180 minutes.

Table 1 summarizes the samples production parameters.

The cross sections of the samples were metallographically prepared and examined by light microscopy (B201, Olympus) and scanning electron microscopy (JSM 6360, Jeol). Energy Dispersive Spectroscopy (EDS) analysis was performed using a Quantax 75 (Bruker Nano GmbH). Porosity values were determined by Archimedes principle³⁴ using a precision balance (EMB, Kern) equipped with a floating device. The obtained results were double-checked by numerical analysis of light microscopy images. Phase composition was analyzed by X-Ray diffraction using Cu K α radiation in a Bruker AXS, D8 Advance diffractometer. Rietveld method using the DIFFRAC.TOPAS (Bruker) software was applied to determine the lattice parameters and estimate the mass portion corresponding to each phase. Differential scanning calorimetry (DSC) analysis were performed in the samples produced by tape casting and sintered at 1200 °C using a Q2000 DSC calorimeter (TA Instruments, USA) equipped

with an RCS refrigeration accessory. N₂ was used as purge gas, and a heating rate of 5 °C min⁻¹ was applied. Vickers Microhardness values were measured in HMV Shimadzu Microhardness tester applying a load of 4.90 N for 15 s following the ASTM E92³⁵. The dynamic Young's modulus (E) was measured by a vibroacoustic technique according to the Pritz method³⁶. Two accelerometers Type 4513-B from Brüel & Kjær (IEPE TEDS), a Brüel & Kjær electrodynamic shaker, Type 4824, and a National Instruments signal acquisition chassis model cDAQ-9171 were used for the experimental characterization and MATLAB software was used for the frequency domain signal postprocess. The compression tests were performed in cylinders of 10 mm diameter and 18 mm height produced from warm compaction of MIM feedstocks. The compression tests were based on ASTM-E9³⁷ and performed at room temperature using an Instron/EMIC23-100 with a speed of 0.018 mm/min.

3. Results and Discussion

Tape casting enabled the production of porous Ti-16Nb sheets of ca. 700 μm from coarse Nb particles ($D_{50} = 110 \mu\text{m}$ and $D_{90} = 255 \mu\text{m}$). Both sintering temperature and Nb particle size had an effect on sintering behavior and, as consequence, in the porosity and microhardness values (Table 2). As expected, by increasing sintering temperature, shrinkage increases and porosity decreases. So that, in the samples sintered up to 1000 °C, a well interconnected porosity was observed, while in the samples sintered at 1100 °C and 1200 °C the pores started to close and the amount of macropores was significantly reduced as shown in the SEM images (Figure 2). On the other hand, larger Nb particle size hindered sintering resulting in lower shrinkage and higher porosity (Table 2).

Table 1. Sample composition and sintering parameters.

Sample Code	Process	Powder load (vol.%)	Powder composition		Sintering Temperature
			Ti	Nb (D_{50})	
Ti16Nb_t900	Tape casting	40	84	16 (110 μm)	900
Ti16Nb_t1000	Tape casting	40	84	16 (110 μm)	1000
Ti16Nb_t1100	Tape casting	40	84	16 (110 μm)	1100
Ti16Nb_t1100_g	Tape casting	40	84	16 (255 μm)	1100
Ti16Nb_t1200	Tape casting	40	84	16 (110 μm)	1200
Ti16Nb_t1200_g	Tape casting	40	84	16 (255 μm)	1200
Ti10Nb_c1200	Warm compaction	60	90	10 (110 μm)	1200
Ti16Nb_c1200	Warm compaction	60	84	16 (110 μm)	1200
Ti22Nb_c1200	Warm compaction	60	78	22 (110 μm)	1200

Table 2. Porosity and Microhardness values of tape casting samples.

Sample	Porosity	Shrinkage in Thickness (%)	Microhardness (HV)
Ti16Nb_t900	30.8 \pm 5.0	6.6	56.5 \pm 8.2
Ti16Nb_t1000	28.9 \pm 2.3	9.3	146.8 \pm 41.2
Ti16Nb_t1100	18.6 \pm 2.1	14.1	249.4 \pm 112.9
Ti16Nb_t1100_g	25.2 \pm 4.0	12.8	218.3 \pm 68.7
Ti16Nb_t1200	14.1 \pm 5.2	15.6	515.5 \pm 148.2
Ti16Nb_t1200_g	18.4 \pm 4.1	15.4	458.5 \pm 96.5

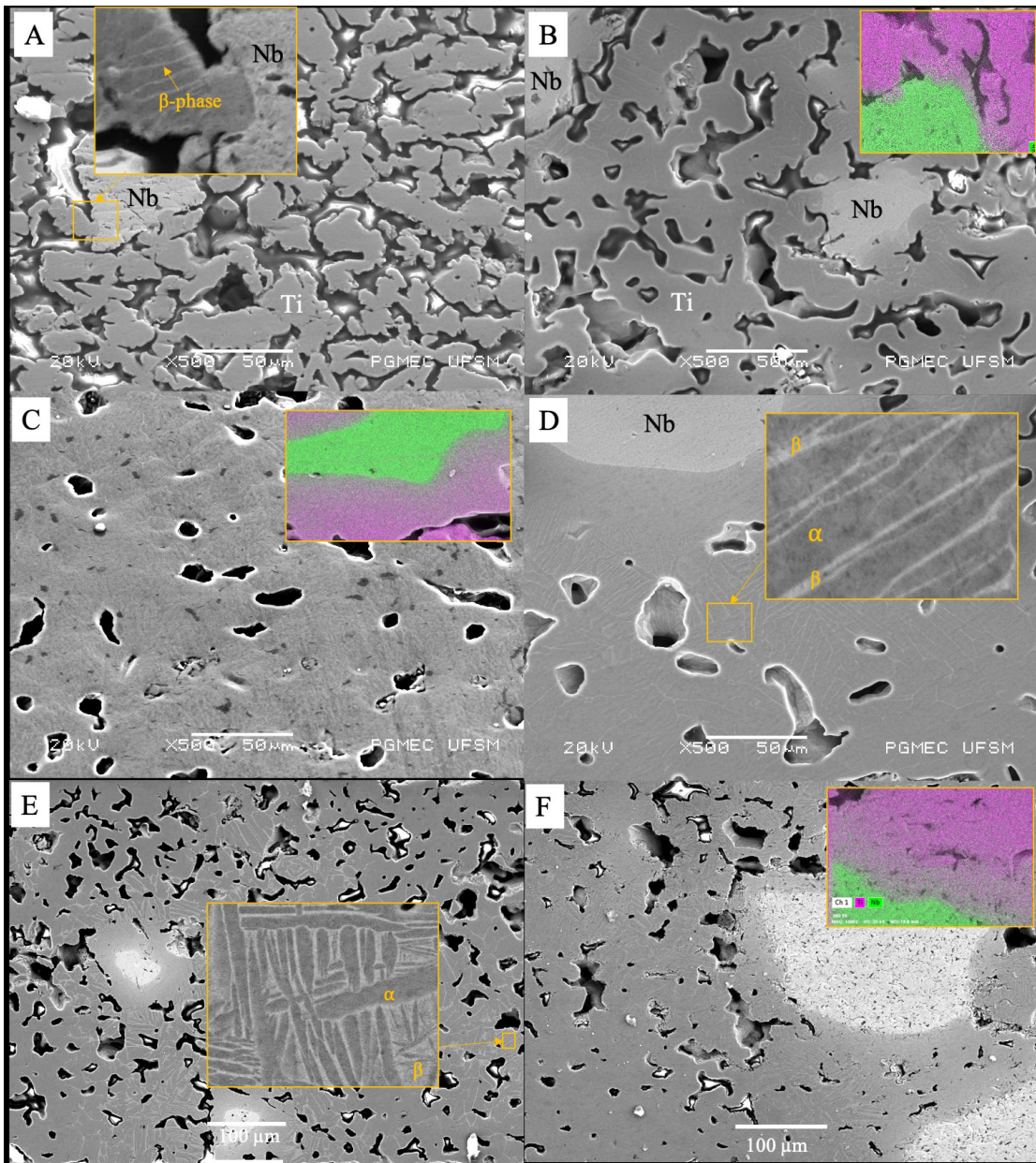


Figure 2. Cross section micrographs of Ti16Nb sheets produced from tape casting: (A) Ti16Nb_t900, (B) Ti16Nb_t1000, (C) Ti16Nb_t1100, (D) Ti16Nb_t1100g (E) Ti16Nb_t1200 and (F) Ti16Nb_t1200g. EDS map of Ti (purple) and Nb (green) are shown in the highlights.

Microhardness values increased with increased sintering temperature (Table 2). As reported in the literature³⁸ the increase in hardness with increasing sintering temperature is mainly related to the reduced porosity and increased Nb diffusion. Reducing particle size had a similar effect to increasing the sintering temperature, due to the greater contact surface area between Ti and Nb particles which increases the diffusion rate. Therefore, the highest microhardness value (515 HV) was found in the samples produced with smaller Nb particles and sintered at a higher temperature. Microhardness values similar to those reported in the literature for cast Ti-Nb binary alloys^{9,14} were achieved in the Ti-Nb sheets sintered at 1100 and 1200 °C.

Ti16Nb tapes sintered at 900 °C (Figure 2A) showed the highest interconnected porosity and the lowest Nb and Ti interdiffusion. The microstructure mainly consists of non-homogeneous distribution of α -Ti grains and Nb grains. Nb particles had a poor dissolution in the Ti matrix, so that the Nb atoms are mostly concentrated where the starting Nb particles were located before sintering. However, the Nb particles are well bonded to the titanium matrix and a small amount of β -phase has been observed around the Nb particle, indicating that, despite being lower, there has been some interdiffusion between Nb and Ti particles. XRD pattern (Figure 3A) corroborates that Ti16Nb_t900 sheets consist mainly of α -Ti and Nb phases, the amount of β -Ti phase being too low to be distinguished by XRD.

By increasing sintering temperature to 1000 °C (Figure 2B), Nb and Ti interdiffusion increased and the porosity decreased; nevertheless, a microstructure with an interconnected porosity and a non-homogeneous distribution of α -Ti and Nb grains with a small amount of β -Ti phase is still observed. As Nb and Ti interdiffusion increases, the amount of β -phase slight increases, however remains too low to be distinguished by XRD (Table 3).

Further increasing sintering temperature to 1100 and 1200 °C promoted a greater interdiffusion between Nb and Ti particles – which can be observed in the SEM images and EDS maps (Figure 2C-F) – as a result, the amount of β -phase and densification are improved (Figure 2C-F), so that peaks related to the β -phase were detected in the XRD patterns (Figure 3 and Table 3). Microstructure of samples sintered at 1100 and 1200 °C consists mainly of α -Ti, β -Ti and Nb phase, as suggested by SEM (Figure 2) and XRD analysis (Table 3). In spite of the better homogenization, Nb particles are still not completely dissolved in the Ti matrix and there is a higher concentration of β -Ti phase where starting Nb particles were located before sintering. Furthermore, an increase in the sintering temperature resulted in a slight increase in the lattice parameters “a” and “c” of the α -Ti phase (Table 3). At higher temperatures, Nb and Ti interdiffusion is enhanced as consequence the β -Ti stability is increased. An increased β -Ti stability can during cooling slow down the β/α transformation potentially leading to distortion in the lattice parameters^{39,40}. XRD patterns (Table 3) also indicated that the amount β -Ti increases with sintering temperature. Furthermore, in contrast with the literature reports for Ti-Nb parts sintered at 1500 °C¹², no carbides precipitation was observed in SEM images or XRD analysis, which can be related to binder composition and relative low sintering temperature²².

As previously mentioned, Nb particle size also had an effect on sintering behavior. Larger Nb particle size decreases the effective surface contact area between Ti and Nb particles hindering diffusion and sintering. So that, Nb and Ti interdiffusion was lower and the microstructure less homogenous in the samples produced with larger Nb particles ($D_{50} = 255 \mu\text{m}$) compared to samples produced with smaller Nb particles ($D_{50} = 110 \mu\text{m}$) and sintered at the same temperature (Figure 2C-F). As a result of the lower interdiffusion between Ti and Nb, the amount of β -phase decreases in the parts produced with larger Nb particles as suggested by XRD analysis (Table 3).

DSC curves of Ti-16Nb sheets produced from the larger Nb particles ($D_{50} = 255 \mu\text{m}$) and the smaller Nb particles ($D_{50} = 110 \mu\text{m}$) and sintered at 1200 °C are shown in Figure 4.

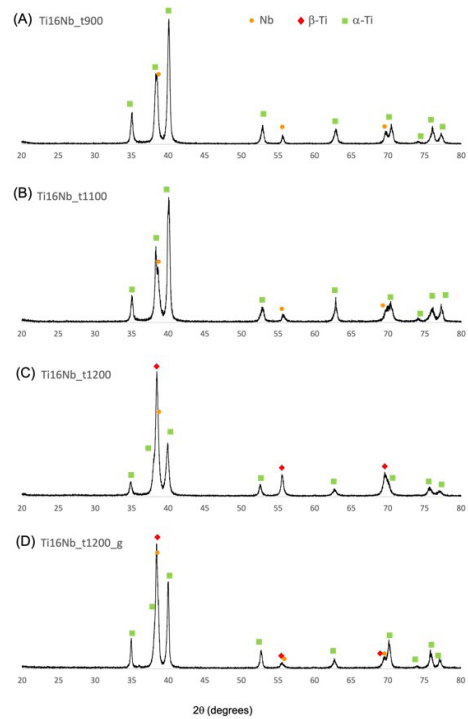


Figure 3. XRD diffraction patterns of Ti16Nb sheets produced from tape casting: (A) Ti16Nb_t900, (B) Ti16Nb_t1000, (C) Ti16Nb_t1200, (D) Ti16Nb_t1200g.

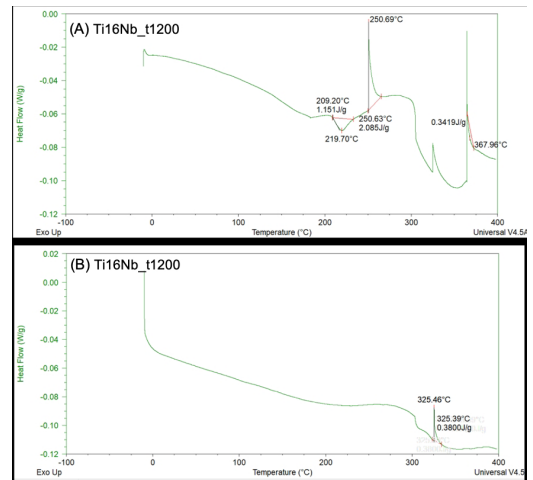


Figure 4. DSC curves of (A) Ti16Nb_t1200, (B) Ti16Nb_t1200g.

Table 3. Lattice parameters and phase composition of Ti16Nb sheets produced from tape casting.

Sample	α -Ti Lattice (Å)		β -Ti Lattice (Å)	Nb Lattice (Å)	Phase Composition (%)		
	a	c			α -Ti	β -Ti	Nb
Reference	2.951	4.682	3.284	3.305	-	-	-
Ti16Nb_t900	2.951	4.682	-	3.307	84.29	-	15.71
Ti16Nb_t1000	2.952	4.692	-	3.322	87.54	-	12.46
Ti16Nb_t1100	2.958	4.696	3.284	3.299	60.98	28.05	10.97
Ti16Nb_t1200	2.968	4.847	3.284	3.311	28.02	65.63	6.34
Ti16Nb_t1200_g	2.964	4.716	3.289	3.316	49.54	38.58	11.88

The Ti-16Nb_t1200 samples with the smaller Nb particles showed an endothermic peak at 219.70 °C and exothermic peaks at 250.69 °C and 367.96 °C, while the sample with larger Nb particles, Ti-16Nb_t1200g, only showed an exothermic peak at 325.46 °C. The exothermic peaks can be related to the precipitation of β - and ω -phases and the endothermic peaks to the precipitation of α -phase as reported by Cremasco et al.⁴¹ and Mantani and Tajima⁴². Coarser Nb particles hinder diffusion so that a smaller amount phase transformations are expected to be observed in the DSC analysis. Further studies are necessary to better understand the effect of particle size on phase transformations.

In summary, reducing Nb particle size and increasing sintering temperature of sheets produced by tape casting favors Ti and Nb interdiffusion, reduces porosity, increases the amount of β -phase, improves hardness and the microstructure homogeneity. For better homogenization of Ti-Nb alloys microstructures, higher sintering temperatures in the range 1300-1350 °C²¹ will be investigated as ongoing of this research. In the case of parts produced with larger Nb particles even higher sintering temperatures and dwell time will be considered to achieved complete homogenization.

In order to obtain a more homogeneous microstructure, the Nb powder with an average particle size of $D_{50} = 110 \mu\text{m}$ and a sintering temperature of 1200 °C were selected for the production of samples by warm compaction of MIM feedstocks.

The Nb particles used in this study are considerable coarse compared to the standard particles used for MIM, which usually have particle size distributions in the range of 5 μm to 40 μm ⁴³. In the warm compacted samples, the amount of Nb varied from 10 to 22 wt.% to produce ($\alpha+\beta$) Ti alloy. When compared to samples produced by tape casting, the samples produced by warm compaction showed a much higher densification which is inherent to the manufacturing process (Table 4) and a more homogeneous microstructure. The porosity values of warm compacted samples were slight lower than those reported in the literature for Ti-Nb alloys with similar compositions produced by MIM^{12,21}.

Microstructural evaluation of warm compacted samples (Figures 5-8) indicates they are formed by ($\alpha+\beta$) microstructure with some regions of higher Nb concentrations, which remain due to incomplete dissolution of the Nb particles into the Ti matrix. The regions with higher concentrations of Nb are brighter in the SEM images due to the higher atomic number of Nb compared to Ti. The EDS maps confirm that some of the brighter regions are rich in Nb (Figure 8A-D), however other brighter regions, despite being relate to the regions where Nb particles were located before sintering, show a homogenous distribution of ($\alpha+\beta$) phases, indicating that Nb particles have been completely dissolved in these regions (Figure 7B-E). Furthermore, EDS maps (Figure 6-8) confirmed that β -phase is rich in Nb, which is expected since Nb is β -stabilizer.

Table 4. Porosity and mechanical properties of the parts produced from warm compaction of MIM feedstocks.

Sample	Porosity (vol%)	Microhardness (HV)	Dynamic Young's Modulus (GPa)	Compressive Yield Strength (MPa)
Ti10Nb_c1200	1.72 ± 0.41	468.8 ± 66.4	37.2 ± 2.2	1014.6 ± 54.6
Ti16Nb_c1200	1.76 ± 0.52	549.2 ± 95.5	49.1 ± 0.2	1100.9 ± 27.4
Ti22Nb_c1200	1.83 ± 0.59	420.6 ± 187.8	51.8 ± 3.1	975.26 ± 54.0

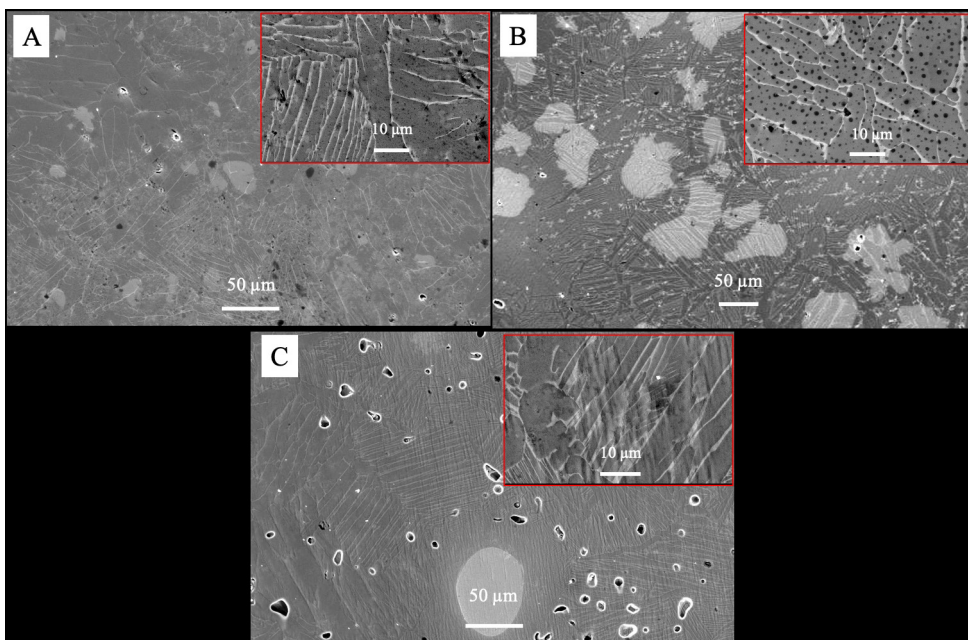


Figure 5. Cross section micrographs of Ti-Nb parts produced from warm compaction of MIM feedstocks: (A) Ti10Nb_c1200, (B) Ti16Nb_c1200, (C) Ti22Nb_c1200.

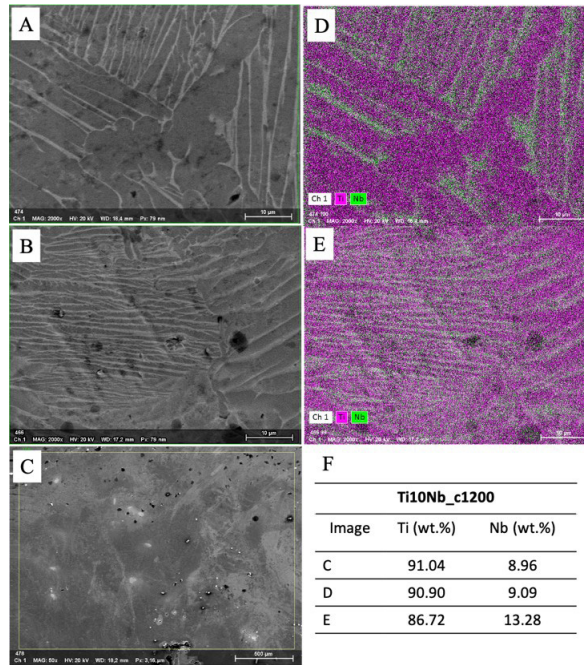


Figure 6. SEM images (A), (B), (C), EDS maps (D), (E) of Ti (purple) and Nb (green) and elemental composition (F) of selected regions of the Ti10Nb_c1200 part.

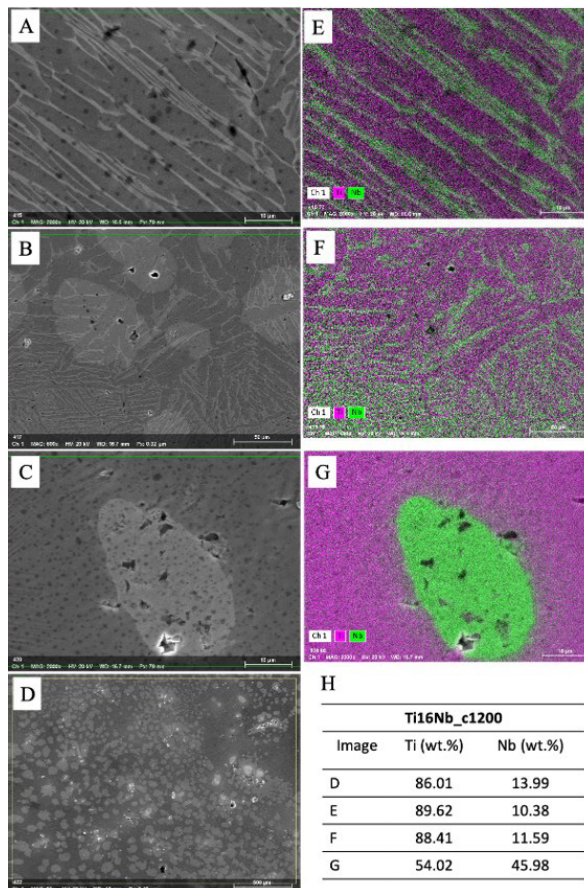


Figure 7. SEM images (A), (B), (C), (D), EDS maps (E), (F), (G) of Ti (purple) and Nb (green) and elemental composition (H) of selected regions of the Ti16Nb_c1200 part.

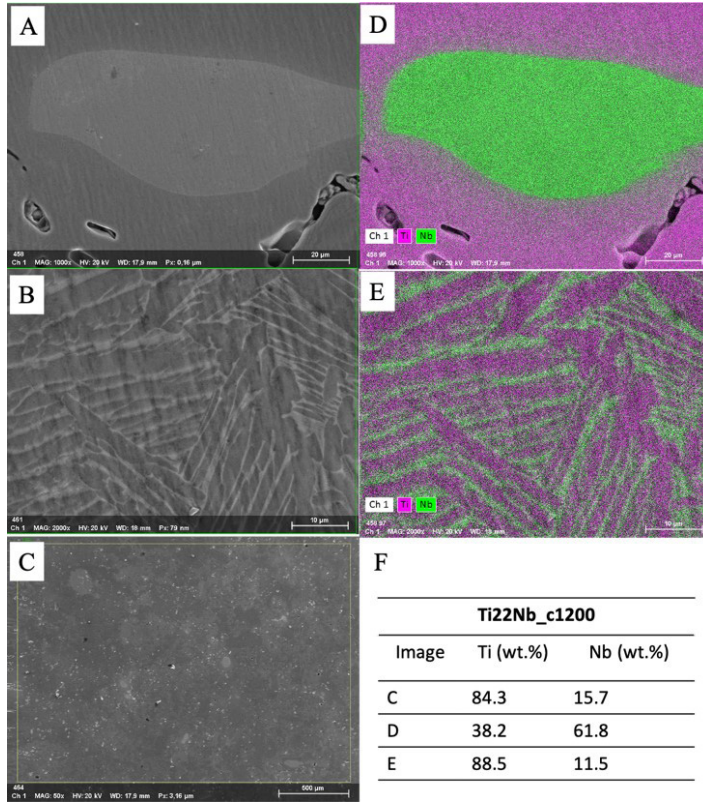


Figure 8. SEM images (A), (B), (C), EDS maps (D), (E) of Ti (purple) and Nb (green) and elemental composition (F) of selected regions of the Ti22Nb_c1200 part.

Ti10Nb and Ti16Nb samples sintered at 1200 °C have Kirkendall porosity (Figure 5), which results from the mismatch between diffusion rates of Ti and Nb. In the Ti22Nb samples, Kirkendall effect was not observed, probably due to the higher concentration of Nb which slows down its diffusion. Kirkendall porosity was also observed by Zhao et al.²¹ in Ti-Nb alloys produced by MIM using finer spherical Ti powders ($D_{50} = 21 \mu\text{m}$) and Nb powders ($D_{50} = 75 \mu\text{m}$).

XRD diffraction patterns (Figure 9, Table 5) indicated that the warm compacted parts are formed by α -Ti and β -Ti phases with some residual Nb phase, being the amount of residual Nb phase higher in the Ti22Nb_c1200 samples due to the higher Nb content, which decreases its diffusivity. A slight increase in the lattice parameters “a” and “c” of the α -Ti phase was also observed, as reported for the tape casting samples (Table 5).

Ti16Nb_c1200 samples, which have a Nb content of 16 wt.% Nb, showed the highest hardness values. The increased hardness of Ti16Nb parts compared to Ti10Nb parts (Nb content of 10 wt.% Nb) can be related to the solid solution strengthening of the α -Ti phase. By increasing Nb content to 22 wt.%, the amount of Nb phase was increased, since the Nb phase has a lower hardness than the solution hardened α -Ti phase, the hardness of Ti22Nb parts was decreased. These results are consistent with the work carried out by Lee et al.¹⁴. Compressive yield strength had the same tendency of microhardness with Ti16Nb_c1200 samples (Nb content of 16 wt.% Nb) showing the highest strength.

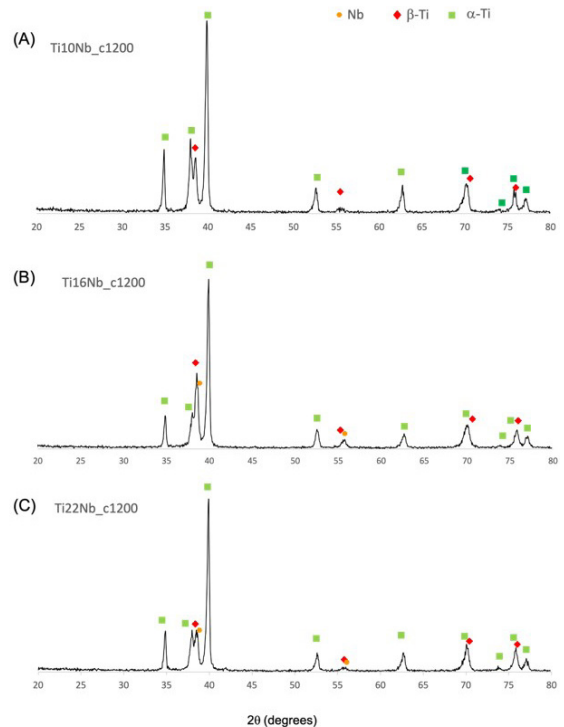


Figure 9. XRD patterns of the samples produced by warm compaction of MIM feedstocks: (A) Ti10Nb_c1200, (B) Ti16Nb_c1200 and (C) Ti22Nb_c1200.

Table 5. Lattice parameters and phase composition of the samples produced by warm compaction of MIM feedstocks.

Sample	α -Ti Lattice		β -Ti Lattice (\AA)	Nb Lattice (\AA)	Phase Composition (%)		
	a (\AA)	c (\AA)			α -Ti	β -Ti	Nb
Reference	2.951	4.682	3.284	3.304			
Ti10Nb_c1200	2.969	4.742	3.299	3.307	73.49	21.22	2.29
Ti16Nb_c1200	2.971	4.727	3.293	3.305	70.52	21.58	7.90
Ti22Nb_c1200	2.968	4.729	3.294	3.307	74.84	16.13	9.03

Compressive yield strength was in the range of 975 to 1000 MPa. Compression tests were performed until maximum load of 70 kN, which resulted in elongation of ca. 15-20%, indicating a plastic behavior. The compressive mechanical properties were similar to those reported in the literature for Ti-Nb based alloys produced from conventional metal powders⁴⁴⁻⁴⁶.

Dynamic Young's modulus of Ti-Nb alloys produced in this study ranged from 37 to 52 GPa, which is considerably lower than the ca. 90 GPa reported in the literature for commercially pure titanium with similar porosity produced by MIM⁴⁷. Young's modulus increased with Nb content in the Nb range investigated in this study (10-22 wt.%) as shown in Table 4. Once Nb is a β -stabilizer, Nb addition in titanium alloys in general is expected to decrease Young's Modulus due to the formation of β -phase. However, in specific ranges, Nb addition can increase Young's modulus due to the precipitation of ω phase. Han et al.⁴⁸ observed an increase in Young's Modulus in the range of ca. 10 wt.% Nb, while Hon et al.⁴⁹ observed in the range between 26 to 34 wt.% Nb. According to Lee et al.¹⁴ small amounts of ω phase can promote a significant increase in the Young's Modulus. Therefore, we attribute the increase in the Young's modulus with increasing Nb content due to a small precipitation of ω phase, which cannot be detected by XRD (due to its very small amount). The precipitation of ω phase can be expected in the Nb-rich regions. Further investigations are required to confirm the precipitation of ω phase and provide an in-depth understanding of phase transformations and their impact on mechanical properties.

4. Conclusions

Powder metallurgical fabrication of ($\alpha + \beta$) Ti-Nb alloys using coarse HDH Nb ($D_{50} = 110 \mu\text{m}$, and $D_{50} = 255 \mu\text{m}$) and HDH Ti ($D_{50} = 22.6 \mu\text{m}$) powders as starting materials was demonstrated. Porous sheets with a well interconnected porosity in the range of 14-32 vol% were produced by tape casting and almost fully dense parts (with a porosity lower than 2 vol%) were produced by warm compaction of MIM feedstocks.

In the tape casting samples, higher sintering temperature resulted in a higher interdiffusion of Nb and Ti, which increased the amount of β -phase, improved microstructure homogenization and decreased porosity. Microhardness was also improved by increasing sintering temperature due to the porosity reduction. The use of larger Nb particles ($D_{50} = 255 \mu\text{m}$) resulted in a less homogenous microstructure and slightly higher porosity, indicating that, for larger Nb particles, higher sintering temperatures and longer dwell time may be required to improve homogenization.

Warm compaction was used instead of MIM due its similarity to MIM process and because it enables parts to be fabricated with small amount of feedstocks. Samples with 10, 16 and 22 wt.% Nb were fabricated, all of which had ($\alpha + \beta$) microstructure with some residual Nb particles. In spite of the not completely homogenous microstructure, the mechanical properties of the warm compacted parts were similar to the properties reported in the literature for Ti-Nb based alloys produced using finer powders. Furthermore, a Young's modulus significantly lower than that of cp-Ti was achieved.

In summary, Ti-Nb based alloys produced from coarse Nb powders show a good combination of mechanical properties and low Young's modulus, making them attractive for engineering applications. Therefore, this study might provide guidance for using coarse Nb particles as starting materials for powder metallurgical development of low-cost Ti-Nb alloys.

5. Acknowledgments

The experimental support of Inácio da Fountora Limberger and Carlos Roberto Cauduro is well acknowledge. Financial support of FAPERGS, CNPq and CAPES are acknowledged.

6. References

- Destefani JD. Introduction to titanium and titanium alloys. In: ASM International. Properties and selection: nonferrous alloys and special-purpose materials. West Conshohocken: ASM International; 1990. p. 586-91.
- Peters M, Kumpfert J, Ward CH, Leyens C. Titanium alloys for aerospace applications. *Adv Eng Mater.* 2003;5(6):419-27.
- Oryshchenko AS, Gorynin IV, Leonov VP, Kudryavtsev AS, Mikhailov VI, Chudakov EV. Marine titanium alloys: present and future. *Inorg Mater: Appl Res.* 2015;6:571-9.
- Zhang LC, Chen LY. A review on biomedical titanium alloys: recent progress and prospects. *Adv Eng Mater.* 2019;21(4):1801215.
- Bidaux JE, Closuit C, Rodriguez-Arbaizar M, Zufferey D, Carreño-Morelli E. Metal injection moulding of low modulus Ti-Nb alloys for biomedical applications. *Powder Metall.* 2013;56(4):263-6.
- Imtiaz M, Rizwan MS, Xiong S, Li H, Ashraf M, Shahzad SM, et al. Vanadium, recent advancements and research prospects: a review. *Environ Int.* 2015;80:79-88.
- Shaw CA, Tomljenovic L. Aluminum in the central nervous system (CNS): toxicity in humans and animals, vaccine adjuvants, and autoimmunity. *Immunol Res.* 2013;56:304-16.
- Liverani E, Rogati G, Pagani S, Brogini S, Fortunato A, Caravaggi P. Mechanical interaction between additive-manufactured metal lattice structures and bone in compression: implications for stress shielding of orthopaedic implants. *J Mech Behav Biomed Mater.* 2021;121:104608.
- Fikeni L, Annan KA, Mutombo K, Machaka R. Effect of Nb content on the microstructure and mechanical properties of binary Ti-Nb alloys. *Mater Today Proc.* 2021;38:913-7.

10. Pitchi CS, Priyadarshini A, Sana G, Narala SKR. A review on alloy composition and synthesis of β -Titanium alloys for biomedical applications. *Mater Today Proc.* 2020;26(Pt 2):3297-304.
11. Ureña J, Tsipis S, Pinto AM, Toptan F, Gordo E, Jiménez-Morales A. Corrosion and tribocorrosion behaviour of β -type Ti-Nb and Ti-Mo surfaces designed by diffusion treatments for biomedical applications. *Corros Sci.* 2018;140(1):51-60.
12. Zhao D, Chang K, Ebel T, Qian M, Willumeit R, Yan M, et al. Microstructure and mechanical behavior of metal injection molded Ti-Nb binary alloys as biomedical material. *J Mech Behav Biomed Mater.* 2013;28:171-82.
13. Metikoš-Huković M, Kwok A, Piljac J. The influence of niobium and vanadium on passivity of titanium-based implants in physiological solution. *Biomaterials.* 2003;24(21):3765-75.
14. Lee CM, Ju CP, Chern Lin JH. Structure-property relationship of cast Ti-Nb alloys. *J Oral Rehabil.* 2002;29(4):314-22.
15. Hussein MA, Azeem MA, Madhan Kumar A, Saravanan S, Ankan N, Sorour AA. Design and processing of near- β Ti-Nb-Ag alloy with low elastic modulus and enhanced corrosion resistance for orthopedic implant. *J Mater Res Technol.* 2023;24:259-73.
16. Jawed SF, Rabadia CD, Khan MA, Khan SJ. Effect of alloying elements on the compressive mechanical properties of biomedical titanium alloys: a systematic review. *ACS Omega.* 2022;7(34):29526-42.
17. Su Y, Liang C, Sun X, Zhang H, Liang Q, Zheng Y, et al. Composition-dependent shuffle-shear coupling and shuffle-regulated strain glass transition in compositionally modulated Ti-Nb alloys. *Acta Mater.* 2023;246(1):118697.
18. Elmay W, Peltier L, Gabrion X, Kubler R, Piotrowski B, Laheurte P, et al. Damping capacity of Ti-Nb shape memory alloys evaluated through DMA and single-impact tests. *Shape Memory and Superelasticity.* 2022;8:349-55.
19. Yang X, Liu CR. Machining titanium and its alloys. *Mach Sci Technol.* 1999;3(1):107-39.
20. Fang ZZ, Paramore JD, Sun P, Chandran KSR, Zhang Y, Xia Y, et al. Powder metallurgy of titanium-past, present, and future. *Int Mater Rev.* 2018;63(7):7-459.
21. Zhao D, Chang K, Ebel T, Nie H, Willumeit R, Pyczak F. Sintering behavior and mechanical properties of a metal injection molded Ti-Nb binary alloy as biomaterial. *J Alloys Compd.* 2015;640(15):393-400.
22. Daudt NF, Hackemüller FJ, Bram M. Manufacturing of Ti-10Nb based metal sheets by tape casting. *Mater Lett.* 2019;37(15):161-4.
23. Sharma B, Vajpai SK, Ameyama K. Microstructure and properties of beta Ti-Nb alloy prepared by powder metallurgy route using titanium hydride powder. *J Alloys Compd.* 2016;656(25):978-86.
24. Terayama A, Fuyama N, Yamashita Y, Ishizaki I, Kyogoku H. Fabrication of Ti-Nb alloys by powder metallurgy process and their shape memory characteristics. *J Alloys Compd.* 2013;577(Suppl 1):S408-12.
25. Xu P, Pyczak F, Yan M, Kong F, Ebel T. Impacts of yttrium on microstructure and tensile properties of biomedical β Ti-Nb-Zr fabricated by metal injection molding. *Mater Sci Eng A.* 2020;792:139816.
26. Xu P, Ebel T, Pyczak F, Willumeit-Römerban R, Yu S. Influence of defects on damage tolerance of Metal-Injection-Molded β titanium alloys under static and dynamic loading. *Powder Metall.* 2022;65(5):354-64.
27. Hackemüller FJ, Borgardt E, Panchenko O, Müller M, Bram M. Manufacturing of large-scale titanium-based porous transport layers for polymer electrolyte membrane electrolysis by tape casting. *Adv Eng Mater.* 2019;21(6):1801201.
28. Lee JK, Lau GY, Sabharwal M, Weber AZ, Peng X, Tucker MC. Titanium porous-transport layers for PEM water electrolysis prepared by tape casting. *J Power Sources.* 2023;559:232606.
29. de Souza Paraiso O F, de Fuccio R Jr, Betz EW. Mining, ore preparation and niobium-based materials production at Araxá, Brazil. *High-Temp Mater Process.* 1993;11(1-4):119-38.
30. Semboshi S, Masahashi N, Konno TJ, Hanada S. Fracture behavior of niobium by hydrogenation and its application for fine powder fabrication. *Metall Mater Trans, A Phys Metall Mater Sci.* 2006;37A:1301-9.
31. Tuncer N, Bram M, Laptev A, Beck T, Moser A, Buchkremer HP. Study of metal injection molding of highly porous titanium by physical modeling and direct experiments. *J Mater Process Technol.* 2014;214(7):1352-60.
32. Daudt NF, Bram M, Cysne Barbosa AP, Alves Jr C. Surface modification of highly porous titanium by plasma treatment. *Mater Lett.* 2015;141:194-7.
33. Köhl M, Bram M, Moser A, Buchkremer HP, Beck T, Stöver D. Characterisation of porous, net-shaped NiTi alloy regarding its damping and energy-absorbing capacity. *Mater Sci Eng A.* 2011;528(6):2454-62.
34. ASTM: American Society For Testing and Materials. ASTM B962: standard test methods for density of compacted or sintered Powder Metallurgy (PM) products using archimedes' principle. West Conshohocken: ASTM International; 2017.
35. ASTM: American Society For Testing and Materials. ASTM E92: standard test method for vickers hardness of metallic materials. West Conshohocken: ASTM International; 2003.
36. Pritz T. Dynamic Young's modulus and loss factor of plastic foams for impact sound isolation. *J Sound Vibrat.* 1994;178(3):315-22.
37. ASTM: American Society for Testing and Materials. ASTM E9: standard test methods of compression testing of metallic materials at room temperature. West Conshohocken: ASTM International; 2009.
38. Vishnu DSM, Sure J, Liu Y, Kumar RV, Schwandt C. Electrochemical synthesis of porous Ti-Nb alloys for biomedical applications. *Mater Sci Eng C.* 2019;96:466-78.
39. Zhang Y, Liu H, Jin Z. Thermodynamic assessment of the Nb-Ti system. *Calphad.* 2001;25(2):305-17.
40. Bönisch M, Stoica M, Calin M. Routes to control diffusive pathways and thermal expansion in Ti-alloys. *Sci Rep.* 2020;10(1):3045.
41. Cremasco A, Andrade PN, Contieri RJ, Lopes ESN, Afonso CRM, Caram R. Correlations between aging heat treatment, ω phase precipitation and mechanical properties of a cast Ti-Nb alloy. *Mater Des.* 2011;32(4):2387-90.
42. Mantani Y, Tajima M. Phase transformation of quenched α'' martensite by aging in Ti-Nb alloys. *Mater Sci Eng A.* 2006;438-440(25):315-9.
43. EPMA: European Powder Metallurgy Association. Introduction to metal injection moulding [Internet]. EPMA; 2018. no. 4 [cited 2023 Nov 3]. Available from: www.epma.com/mim
44. Nazari KA, Nouri A, Hilditch T. Mechanical properties and microstructure of powder metallurgy Ti-xNb-yMo alloys for implant materials. *Mater Des.* 2015;88:1164-74.
45. Çakmak Ö, Kaya M. Effect of sintering procedure on microstructure and mechanical properties of biomedical TiNbSn alloy produced via powder metallurgy. *Appl Phys, A Mater Sci Process.* 127:561.
46. Kalita D, Czepe T, Wojcik A, Kolano-Burian A, Zackiewicz P, Kania B et al. Microstructure and mechanical properties of Ti-Nb alloys prepared by mechanical alloying and spark plasma sintering. *J Mater Eng Perform.* 2020;29:1445-52.
47. Nyberg E, Miller M, Simmons K, Weil KS. Microstructure and mechanical properties of titanium components fabricated by a new powder injection molding technique. *Mater Sci Eng C.* 2005;25(3):336-42.
48. Han MK, Kim JY, Hwang MJ, Song HJ, Park YJ. Effect of Nb on the microstructure, mechanical properties, corrosion behavior, and cytotoxicity of Ti-Nb alloys. *Materials (Basel).* 2015;8:5986-6003.
49. Hon YH, Wang JY, Pan YN. Composition/phase structure and properties of titanium-niobium alloys. *Mater Trans.* 2003;44:2384-90.